Available online at www.sciencedirect.com
ScienceDirect
Journal of Hydrodynamics
www.sciencedirect.com/
science/journal/10016058

A 3D numerical study of solitary wave interaction with vertical cylinders using a parallelised Particle-In-Cell solver

Qiang Chen[1], Jun Zang[1*], David M. Kelly[2], Aggelos S. Dimakopoulos[3]
[1]WEIR Research Unit, Department of Architecture and Civil Engineering, University of Bath, Bath, UK
[2]Coastal Research Lab., International Hurricane Research Center, Florida International University, Miami, USA
[3]HR Wallingford, Wallingford, Oxon, UK
[*] E-mail: J.Zang@bath.ac.uk

ABSTRACT

This paper aims to provide a better understanding of the interaction between solitary waves and vertical circular cylinders. This is achieved via process based numerical modelling using the parallel Particle-In-Cell based incompressible flow solver PICIN. The numerical model solves the Navier-Stokes equations for free-surface flows and incorporates a Cartesian cut cell method for fluid-structure interaction. Solitary waves are generated using a piston-type wave paddle. The PICIN model is first validated using a test case that involves solitary wave scattering by a single vertical cylinder. Comparisons between the present results and experimental data show good agreement for the free surface elevations around the cylinder and the horizontal wave force on the cylinder. The model is then employed to investigate solitary wave interaction with a group of eleven vertical cylinders. The wave run-up and wave forces on the cylinders are discussed.

KEY WORDS: CFD; hybrid Eulerian-Lagrangian; Particle-In-Cell; solitary wave; vertical cylinder.

INTRODUCTION

Over the past few decades, Computational Fluid Dynamics (CFD) modelling has become very popular in the coastal and offshore engineering community. Both Eulerian grid based models (e.g. the OpenFOAM® model [1]) and Lagrangian particle based models (e.g. the SPHysics model [2]) have been widely used. While the Eulerian method is relatively efficient and better at enforcing boundary conditions for fluid-structure interaction via use of a grid, the Lagrangian method is more suited to handling large free-surface deformations using particles. In an attempt to combine these advantages, the Particle-In-Cell (PIC) method [3-5] is devised by a joint use of grid and particles. In recent years, the PIC method has been introduced to the coastal and offshore engineering field [6-9], where modelling complex wave-structure interaction with computational efficiency remains an important challenge.

The PIC method based solver PICIN has achieved promising results in terms of modelling complex free-surface flows and the interaction of such flows with coastal and offshore structures [7-9]. The PICIN model solves the incompressible Navier-Stokes equations (NSE) for free-surface flows and employs both a tailored Distributed Lagrange Multiplier (DLM) method (see Kelly et al. [7]) and a Cartesian cut cell based two-way strong coupling algorithm (see Chen et al. [9]) for fluid-structure interaction. The novelty of the PICIN model lies in the fact that the linear non-advection terms of the NSE are resolved on an underlying grid, while the nonlinear advection terms are handled using particles in a Lagrangian manner. This makes the model both efficient and flexible in terms of simulating complex physical problems. One the other hand, the double-grid nature of the PIC method makes the model very demanding in memory storage which makes its application in three spatial dimensions particularly challenging. Very recently, the PICIN model was extended to three spatial dimensions and parallelised using the Message Passing Interface (MPI) approach [10]. In this approach the computational domain is decomposed into sub-domains based on the underlying grid and the particles are allowed to move through the sub-domains, assigning the computational loads to each process. This enables the PICIN model to practically simulate 3D problems that arise in the coastal and offshore engineering field.

In this paper, the 3D parallel PICIN model is applied to simulate solitary wave interaction with vertical circular cylinders.

This topic has practical importance as vertical cylindrical structures are widely employed as foundations for coastal and offshore structures; examples include the design of oil platforms, offshore wind turbine foundations and piled wharfs. In the literature, a number of numerical models have been applied to study the interaction of solitary wave and vertical cylinders in different configurations. Yates and Wang [11] studied solitary wave scattering by a single vertical cylinder using the generalized Boussinesq (GB) model and also a physical experiment. Zhao et al. [12] also solved a set of GB equations using a finite element method to simulate nonlinear solitary wave scattering by an array of four vertical cylinders in a square arrangement. Ai and Jin [13] studied a similar configuration of four cylinders but used a non-hydrostatic finite volume model to solve the incompressible NSE. Mo and Liu [14] solved the Euler equations coupled with a volume of fluid (VOF) method for free-surface tracking to simulate a non-breaking solitary wave interacting with a group of three cylinders. In these papers, the principal variables of interest were wave run-up, wave forces and free-surface elevations in the vicinity of the cylinders. In this paper, the PICIN model is first validated using a test case of solitary wave scattering by a single cylinder, in terms of the above-mentioned quantities. Then, the model is applied to an extension study of solitary wave interaction with a group of eleven cylinders, which could be considered as the foundations of column-supported structures [15].

1 NUMERICAL MODEL

The 3D PICIN model solves the incompressible NSE for single-phase flow:

$$\nabla \cdot \boldsymbol{u} = 0 \qquad (1)$$

$$\frac{\partial \boldsymbol{u}}{\partial t} + (\boldsymbol{u} \cdot \nabla)\boldsymbol{u} = \nu \nabla^2 \boldsymbol{u} - \frac{1}{\rho}\nabla p + \boldsymbol{f} \qquad (2)$$

where, in 3D, $\boldsymbol{u}$ is the velocity field; t is the time; p is the pressure; $\boldsymbol{f}$ = (0.0, 0.0, -9.81 m/s^2) corresponds to the gravity acceleration; ρ and ν are the density and kinematic viscosity of the fluid, respectively. As a PIC based solver, the PICIN model employs both Lagrangian particles and an Eulerian grid. The grid is uniform and staggered following Harlow and Welch [16] and eight particles are initially seeded in each fluid cell. Following the full particle PIC approach used in Brackbill and Ruppel [4], the particles are assigned with the mass and momentum of the fluid, and are used to solve the nonlinear advection term (the second term on the left hand side of Eq. 2) and track the fluid configuration (including the free surface), while the underlying grid is solely employed for computational convenience for solving the non-advection terms. During each computational cycle, the non-advection terms are first solved on the grid and then the velocity field carried by the particles and the particle position are updated using the information on the grid; more details of the solution procedure are described in what follows. It is noted that no turbulence models are currently incorporated in the PICIN model.

The overall solution is divided into two major steps: an Eulerian step and a Lagrangian step. In the Eulerian step, the NSE, ignoring the nonlinear advection term, are solved on the grid using the pressure projection technique [17], where a pressure Poisson equation (PPE) is resolved incorporating the boundary conditions. On the free surface boundary, a second-order accurate technique following Gibou et al. [18] is employed to enforce this condition:

$$p = 0 \qquad \text{on } \zeta \qquad (3)$$

where ζ represents the free surface position on the grid that is computed based on the particle position at each time step (see details in Chen et al. [9]). On the solid boundary, a Cartesian cut cell based approach following Ng et al. [19] is used to resolve the following conditions:

$$\boldsymbol{n} \cdot \boldsymbol{u} = \boldsymbol{n} \cdot \boldsymbol{U}_b \text{ and } \boldsymbol{n} \cdot (\Delta t \rho^{-1} \nabla p) = \boldsymbol{n} \cdot \left(\boldsymbol{U}_b^* - \boldsymbol{U}_b^{n+1} \right) \text{ on } \Gamma \qquad (4)$$

where Γ represents the surface of solid objects; $\boldsymbol{n}$ is the unit outward normal vector; $\boldsymbol{U}_b$ is the velocity imposed on the surface of solid objects; the superscript n+1 represents the time step; $\boldsymbol{U}_b^*$ denotes the tentative boundary velocity before the pressure projection step. Once the Eulerian step is completed, a divergence-free velocity field $\boldsymbol{u}^{n+1}$ is obtained on the grid. The velocity change, $\boldsymbol{a}^{n+1} = \boldsymbol{u}^{n+1} - \boldsymbol{u}^n$, on the grid is interpolated, using a 4$^{\text{th}}$-order accurate weighted essentially non-oscillatory (WENO) scheme [20], to increment the velocity field carried by the particles. It is noted that for the purpose of numerical stability, the divergence-free velocity itself, $\boldsymbol{u}^{n+1}$, is also interpolated using the WENO scheme to constitute a small proportion of the final velocity carried by the particles (see more

details in Chen et al. [9]). After the particle velocity field is updated, the remaining advection term of the NSE is solved in the Lagrangian step by advecting the particles. That is, the particles, carrying the updated velocity field, are advected through the divergence-free velocity field on the grid using the 3rd-order accurate Runge-Kutta scheme [21]. Once this is done, one computational cycle is completed. It is noted that at the beginning of the next computational cycle, the velocity field is mapped from the particles to the grid using a SPH-like kernel interpolation that conserves the mass and momentum (see more details in Chen et al. [10]). The current 3D PICIN model also employs the domain decomposition based MPI approach for parallelisation [10]. For full details of the PICIN model, the reader is referred to Kelly et al. [7], Chen et al. [9, 10] and Chen [22].

The solitary wave is generated using a piston-type wavemaker approach following Wu et al. [23, 24]. This approach adopts the formula of wave paddle motion proposed by Goring [25] and combines it with the 9th-order solitary wave solution of Fenton [26]. Specifically, with the assumption that the average horizontal water particle velocity, adjacent to the wave paddle, equals the wave paddle velocity, the motion of the wave paddle is expressed by:

$$\frac{d\xi}{dt} = \frac{C\eta\big|_{x=\xi}}{h+\eta\big|_{x=\xi}} \qquad (5)$$

where ξ is the position of the wavemaker; h is the still water depth; C is the wave celerity and η is the water surface elevation. The water surface elevation η at the wavemaker position is specified according to the 9th-order solitary wave solution of Fenton [26]:

$$\eta\big|_{x=\xi} = h\sum_{i=1}^{9}\eta_i\left(\frac{H}{h}\right)^i \qquad (6)$$

where H is the targeted wave crest height of a solitary wave and η_i is a function of $S = \mathrm{sech}(KX)$, where

$$X = \xi - Ct - \xi_0 \qquad (7)$$

$$K = \sqrt{\frac{3H}{4h^3}}\left(1.0+\sum_{i=1}^{8}K_i\left(\frac{H}{h}\right)^i\right) \qquad (8)$$

$$C^2 = gH\left(1.0+\sum_{i=1}^{9}C_i\left(\frac{H}{h}\right)^i\right) \qquad (9)$$

where ξ_0 is the initial position of the wave crest, which must be a negative value as the solitary wave is generated in a quiescent water flume; K_i and C_i are coefficients; the formulas required to determine η_1 to η_9, K_1 to K_8 and C_1 to C_9 are listed in Table 1 of Fenton [26] and are not repeated here.

In the numerical simulation, the water surface elevation at a certain location is computed as the highest position of the particles around the location in the z-direction. The wave force on a cylinder is calculated by integrating the water pressure over the wetted area of the surface of the cylinder:

$$\boldsymbol{F} = -\int_{\Gamma}\boldsymbol{n}p\,d\Gamma \qquad (10)$$

where $\boldsymbol{n}$ is the unit outward normal vector.

2 RESULTS AND DISCUSSIONS

In this section, the 3D parallel PICIN model is first validated against a benchmark test of solitary wave scattering by a single circular cylinder in terms of wave elevations around the cylinder and the horizontal wave force on the cylinder. After that, the results of an extension study of solitary wave interaction with a group of eleven cylinders are discussed.

2.1 Solitary Wave Scattering By a Vertical Circular Cylinder

In this section, the solitary wave scattering by a single vertical circular cylinder is simulated in order to validate the current numerical model. This test case was previously studied by Yates and Wang [11] through both physical experiments and numerical simulations using a GB model. The experiments conducted by Yates and Wang [11] used a water tank measuring 7.6 m long, 0.76 m wide and 0.6 m deep. The water depth in the experiments was h = 0.04 m. The surface-piercing vertical circular cylinder was placed on the bottom of the water tank and on the centre line of the water tank, and the radius of the cylinder was R = 0.0635 m. The solitary waves used in the experiment were generated by moving a flat plate which filled the tank cross section. The principal variables of interest in this test case were the water surface elevations in the vicinity of the cylinder and the horizontal wave loading on the cylinder. The water surface elevation was measured in a semi-circular region around the cylinder and the location of the measuring point is expressed in the polar angle θ and the radial distance r/R measured from the centre of the cylinder. As examples, θ = 0° represents the upstream centre line of the water tank and r/R = 1.0 is on the surface of the cylinder. Fig. 1 shows a sketch of the arrangement of the measuring points.

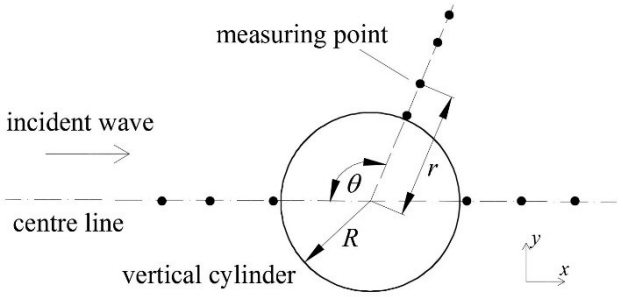

Fig. 1 Sketch of the arrangement of the measuring points for the water surface elevation

A numerical wave tank (NWT) was established for the present simulation. While the width of the NWT was the same as that of the water tank in the experiment, the length of the NWT was reduced to 2.0 m in order to save on CPU cost. The solitary wave was generated using the approach described in Section 1 by a piston-type wavemaker which was located at the upstream end of the NWT, and for all test cases in this section, ξ_0 in Eq. 7 was set to -0.5 m. The cylinder was placed at the centre line of the NWT in the x-direction with the distances to the wavemaker being 1.0 m and to the downstream end of the NWT being 0.95 m, respectively. The grid size was set to $\Delta x = \Delta y = \Delta z$ = 0.0016 m, resulting in approximately 114.89 million particles and 29.86 million grid cells (note that the height of the NWT was set to 0.08 m). The Courant number was set to 0.5. It took approximately 20.8 hours for a non-dimensional $t(g/h)^{1/2}$ = 78.3 of simulation time with 80 cores at the University of Bath High Performance Computing (HPC) system for the test case where the relative wave height was H/h = 0.4.

Fig. 2 shows snapshots of the present numerical results at various time instants for H/h = 0.4. From Fig. 2 it can been seen that as the solitary wave impacts on and passes the cylinder, significant wave run-up occurs and a small positive reflected wave starts to propagate radially outward (see Fig. 2(a)~(c)). This reflected radial wave, as also noted in Yates and Wang [11], diminishes in amplitude as it expands and is followed by a negative wave which develops into oscillatory waves (see Fig. 2(d)~(f)). It is also observed that when the main wave passes, a diffracted wave around the cylinder from the leeward side occurs, which wraps around the cylinder and propagates radially outward (see Fig. 2(d)~(f)). This is consistent with the findings discussed in Yates and Wang [11].

Fig. 3 shows comparisons of the free surface elevation along θ = 0° at different radial positions for H/h = 0.4. Note that in all comparisons of the free surface elevation (including those in Figs. 4 and 5), the time was shifted consistently so that the peak wave amplitude of the numerical result coincides with that of the experimental measurement at r/R = 4.5 and θ = 0°. It can be seen from Fig. 3 that generally the comparisons show good agreement between the present results and the numerical and experimental results obtained by Yates and Wang [11]. In particular, the good agreement of the main wave as shown at r/R = 4.5 demonstrates that the solitary wave is correctly generated in the present simulation. It is nevertheless noted that both numerical models over-predict the maximum wave height very close to the cylinder surface (see r/R = 1.03). We found that this is also the case for the results computed by other numerical models; e.g., Zhao et al. [12], Ai and Jin [13] and Cao and Wan [27]. The secondary wave peak clearly seen at r/R = 2.61 and r/R = 4.5 is due to the reflected wave as observed in Fig. 2.

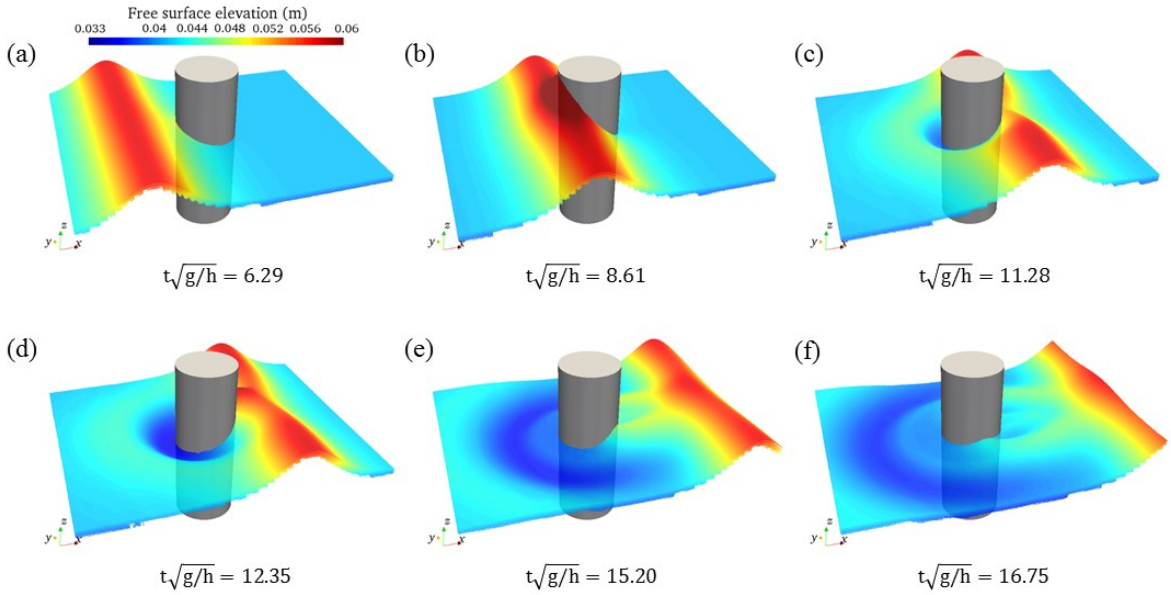

Fig. 2 Snapshots of the present numerical results for $H/h = 0.4$.

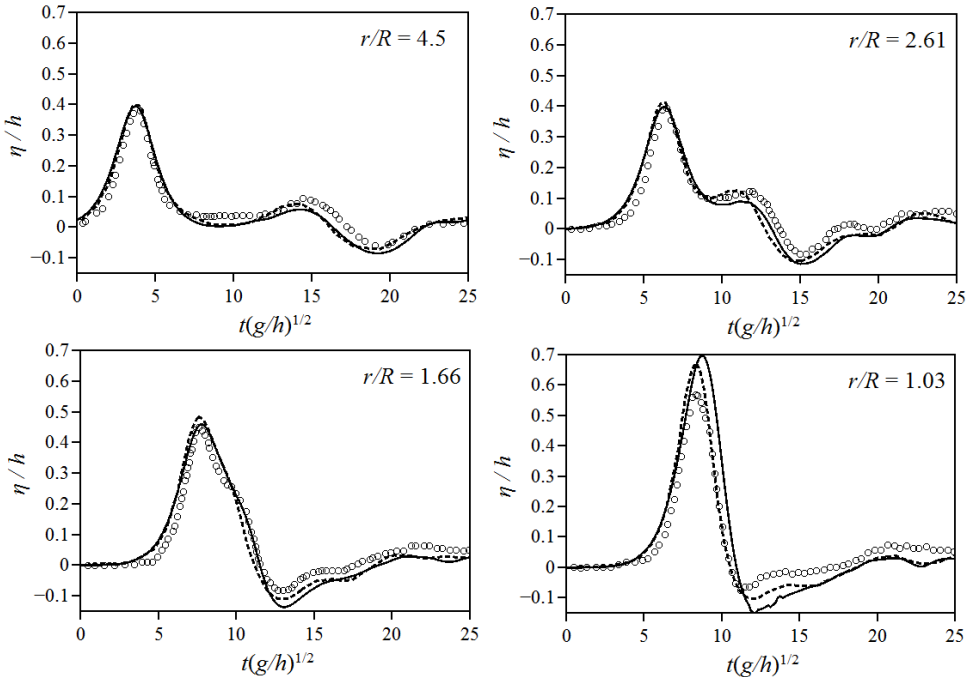

Fig. 3 Comparisons of the time histories of free surface elevation along $\theta = 0°$ at various radial positions: (o), experimental data [11]; (---), numerical results by Yates and Wang [11] and (—), PICIN. The numerical results are for $H/h = 0.4$.

Fig. 4 shows the comparisons of free surface elevation for $\theta = 100°$. The comparisons also show very good agreement between the present results and those obtained by Yates and Wang [11]. Both numerical models again appear to overestimate the main wave peak very close to the surface of the cylinder (see $r/R = 1.03$). However, the present result seems to be slightly better than that of the GB model by Yates and Wang [11]. The secondary wave peak as shown at all radial positions along $\theta = 100°$ is attributed to the diffracted wave from the leeward side of the cylinder rather than the reflected wave. This is confirmed by Fig. 2(e) and (f). That is, as this diffracted wave wraps around the cylinder and propagates radially upstream, along the $\theta = 100°$ line it is first observed at $r/R = 1.03$ and 1.35 at around $t(g/h)^{1/2} = 16$, and then observed at other radial points after a small time lag.

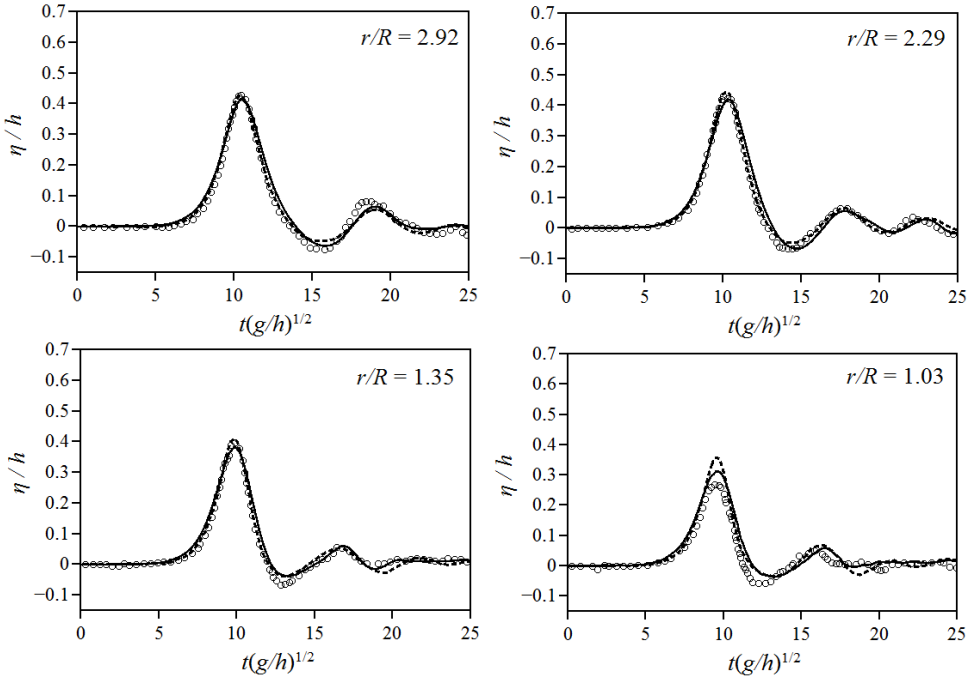

Fig. 4 Comparisons of the time histories of free surface elevation along $\theta = 100°$ at various radial positions: (o), experimental data [11]; (---), numerical results by Yates and Wang [11] and (—), PICIN. The numerical results are for $H/h = 0.4$.

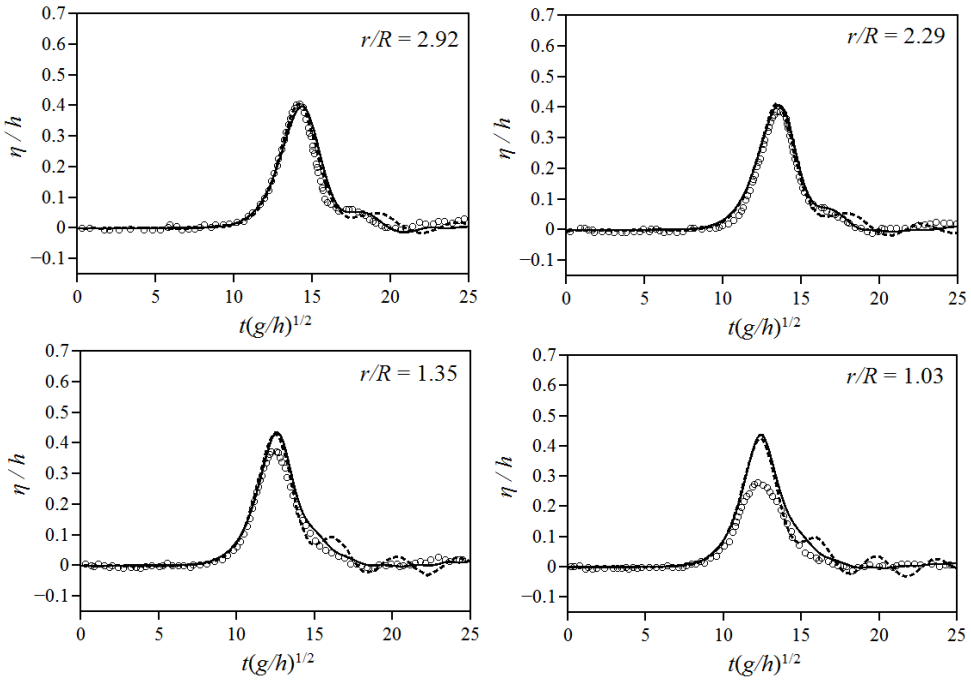

Fig. 5 Comparisons of the time histories of free surface elevation along $\theta = 180°$ at various radial positions: (o), experimental data [11]; (---), numerical results by Yates and Wang [11] and (—), PICIN. The numerical results are for $H/h = 0.4$.

Fig. 5 shows the comparisons of free surface elevation along the downstream centre line $\theta = 180°$. Again, reasonable agreement between the present results and those obtained by Yates and Wang [11] is shown. Note that the main wave peak in the experiment is significantly reduced very close to the surface of the cylinder and both the numerical models over-predict the wave amplitude. Similar results can also be found in the numerical model of Zhao et al. [12].

In Fig. 6, comparisons of the horizontal wave force are shown for various relative wave heights. For each case, the time is shifted such that the peak of the wave force of the present numerical result coincides with that of the experimental measurement. It can be seen from Fig. 6 that for small amplitude waves (see $H/h = 0.24$), the present

numerical result agrees well with the experimental data. However, the discrepancy between the numerical and the experimental data becomes larger when the wave amplitude increases. In general, the present numerical results are in reasonable agreement with the experimental measurements.

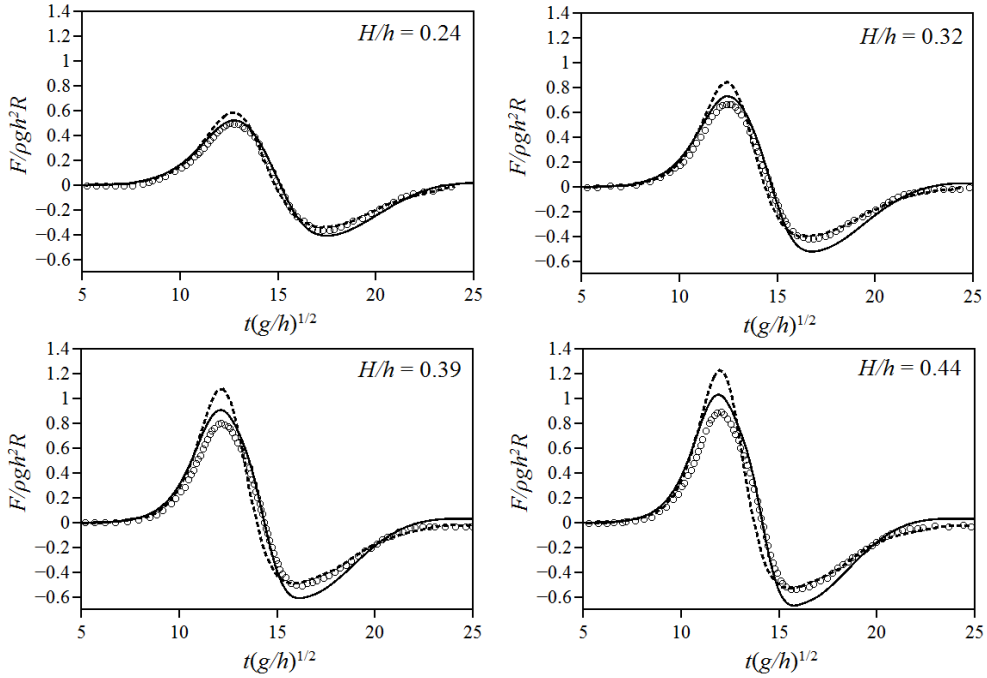

Fig. 6 Comparisons of the time histories of the horizontal wave force for various incident wave heights: (o), experimental data [11]; (---), numerical results by Yates and Wang [11] and (—), PICIN.

2.2 Solitary Wave Interacting With a Group of Cylinders

This section presents an extension study of solitary wave interaction with a group of eleven cylinders. The principal variables of interest in this test case are the wave run-up, R, at the front stagnation point of each cylinder and the horizontal wave forces, F, on the cylinders. The properties of the solitary wave and the layout of the cylinders used in this test case are inspired by those proposed in Mo and Liu [14]. Fig. 7 shows a sketch of the arrangement of the eleven vertical circular cylinders and the setup of the NWT. The cylinders are labelled with C1, C2, etc. (see Fig. 7) and have an identical diameter D. They are symmetrically placed on the centre line of the NWT, with the centre-to-centre distances being $2D$ between the adjacent cylinders in both the streamwise and the spanwise directions (see Fig. 7). The distance in the x-direction between the centre of cylinder C1 and the wavemaker was $14.7D$. The length and the width of the NWT were set to $28.71D$ and $9.93D$, respectively, and the water depth, h, was fixed at $0.615D$. A piston-type wave paddle was employed at the upstream end of the NWT as shown in Fig. 7 for solitary wave generation using the approach described in Section 1. The solitary wave used in this test case was non-breaking; the relative wave height H/h was 0.4 and ξ_0 in Eq. 7 was set to $-6.563D$.

The grid size used in the numerical modelling was $\Delta x = \Delta y = \Delta z = 0.04h$, resulting in approximately 88.75 million particles and 31.37 million grid cells (note that the height of the NWT was set to $1.64D$). The Courant number was 0.5. It took approximately 14.2 hours for a non-dimensional $t(g/h)^{1/2} = 54$ of simulation time with 160 cores at the University of Bath HPC system for this demanding test case.

Fig. 8 shows snapshots of the simulated wave field in plan view at different time instants. The solitary wave travels from left to right. Generally, it is seen that as the solitary wave passes the cylinders, circular scattered waves start to propagate radially away from the cylinders, which are similar to what was observed in the single cylinder case presented in Section 2.1. Focusing more on detail, it can be seen from Fig. 8(b) that a steep wave (maybe close to breaking) forms in front of the cylinders C5 and C6 due to the symmetric scattered waves from both cylinders interacting with each other and propagating upstream. However, as seen from Fig. 8(d), similar waves emanating from cylinders C2 and C3 are blocked by cylinder C4, and the waves could be reflected back and trapped in the cylinder group C1-C2-C3-C4. Moving to Fig. 8(f), it is seen that after the solitary wave completely passes the cylinder group, a complex wave field has formed, due to both wave-wave and wave-structure interaction.

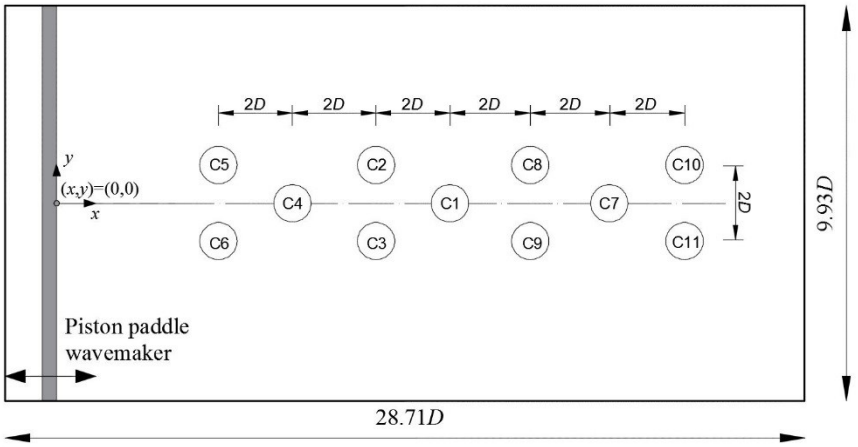

Fig. 7 Sketch (plan view) showing locations of the eleven cylinders in the NWT. D is the diameter of the cylinders.

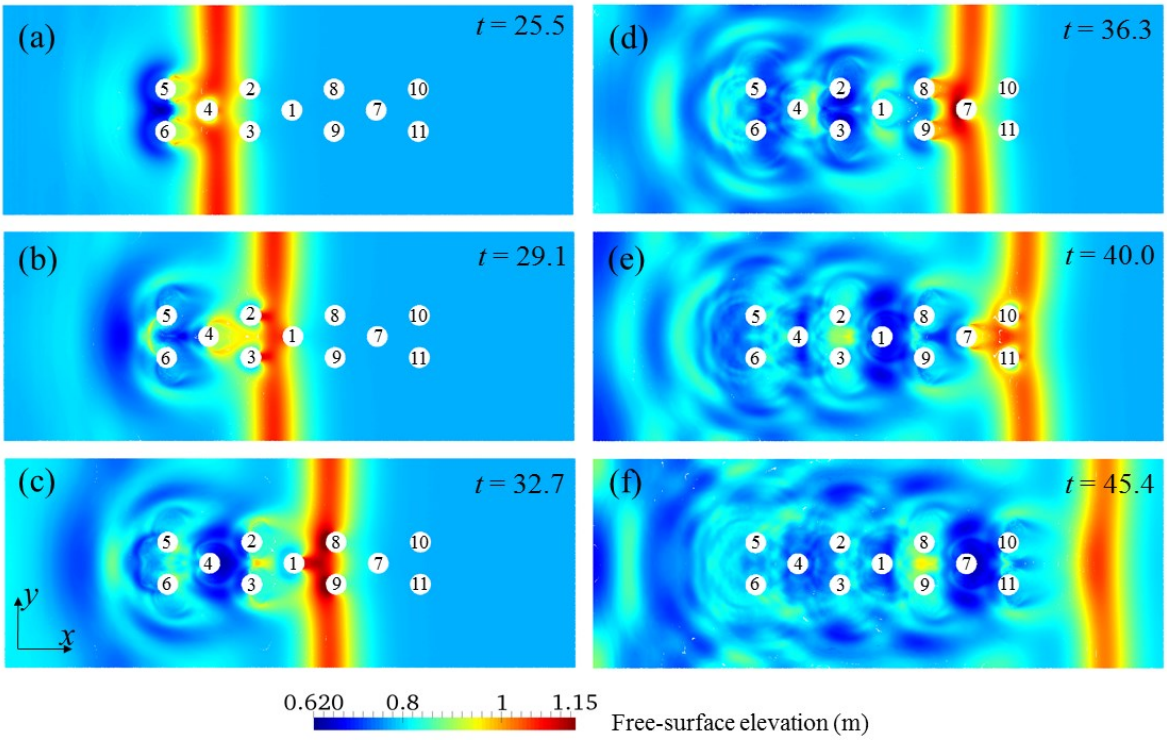

Fig. 8 Snapshots (plan view) of the numerical simulation of a solitary wave interacting with a group of eleven cylinders. t is the simulation time normalised by $(h/g)^{1/2}$.

The numerical results of the wave run-up R at the upstream stagnation points of the cylinders and the wave force F on the cylinders are plotted in Fig. 9. Since the flow field is symmetrical, the results are presented for two cylinder groups based on their positions: the first group consists of cylinders C1, C4 and C7, which are located in the middle, and the second group includes cylinders C2, C5, C8 and C10, which are located at the leftmost side (facing downstream). The results were all shifted in time, with the time instants of all main peak values made to coincide with the non-dimensional time zero.

Fig. 9(a) shows the results for wave run-up. It can be seen that all cylinders in the first group (located in the middle) exhibit very similar wave run-up for this spatial configuration of cylinders. Similar run-up is also observed at the lateral cylinders C2, C8 and C10, with the exception of cylinder C5, which is located at the front of the cylinder group. Both the primary and the secondary peaks of the wave run-up at cylinder C5 appear to be the largest. In particular, the very steep secondary peak wave confirms the observations in Fig. 8(b).

Fig. 9(b) presents the results for the horizontal wave forces on the cylinders. It is seen that the horizontal wave forces are nearly identical on all the three middle cylinders until the secondary force peaks. These secondary peak values are approximately 38% of their corresponding primary peak values. For the forces on the lateral cylinders, cylinder C5 again encounters the largest wave forces for both the primary peak and the primary trough. Apart from these, the secondary peak forces on all lateral cylinders are very close and are nearly 20% of their corresponding primary peak forces.

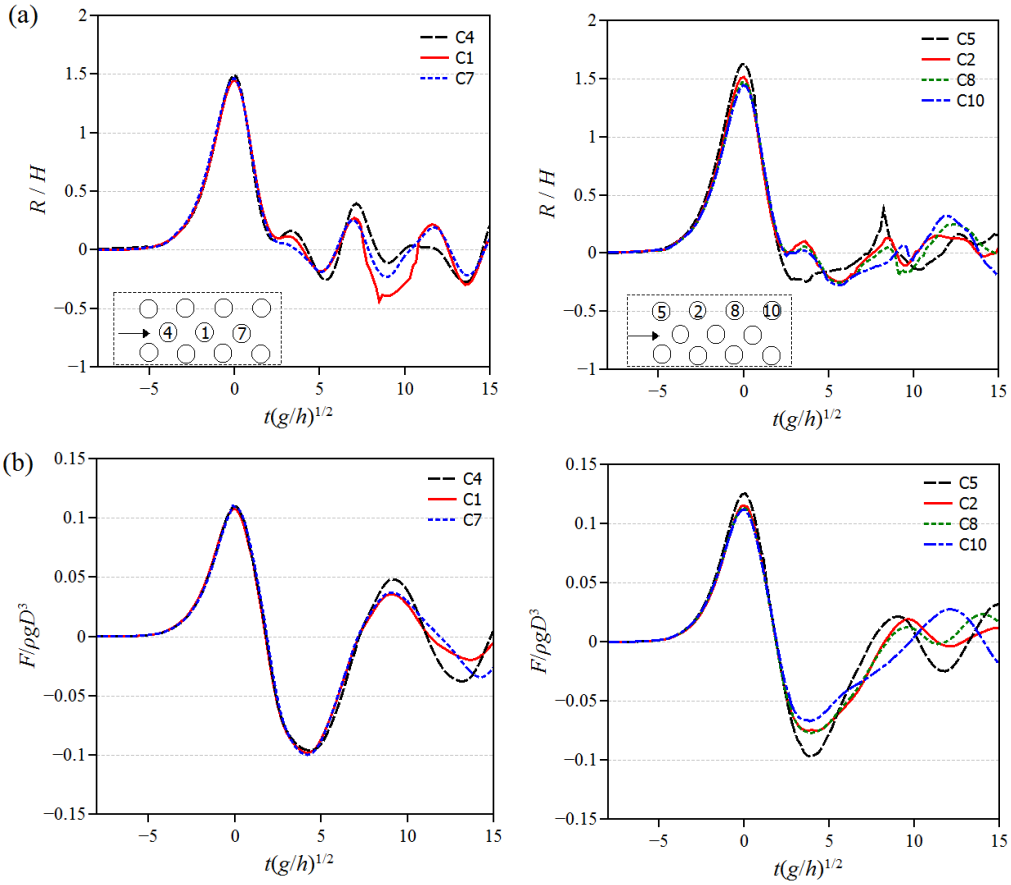

Fig. 9 Comparisons of the numerical results: (a) wave run-up at the upstream stagnation points of different cylinders; (b) horizontal wave forces on the cylinders.

3 CONCLUSIONS

Solitary wave scattering by vertical circular cylinders has been simulated using the 3D parallel PICIN model in this paper. The 3D PICIN model employs the hybrid Eulerian-Lagrangian PIC method to solve the incompressible Navier-Stokes equations (NSE) for free-surface flows and incorporates a Cartesian cut cell based approach for fluid-structure interaction. Due to the PIC nature, both Lagrangian particles and an Eulerian grid are employed in the PICIN model; the particles carry all the material information of the fluid, and are used to track the free surface and solve the nonlinear advection term in the NSE, while the underlying grid is solely employed for computational convenience in solving the non-advection terms of the NSE. Parallelisation based on the MPI approach has also been implemented which enables the PICIN model to the simulation of large-scale 3D problems (i.e. those require a large number of grid cells and particles). The numerical model was first validated using the test case of solitary wave scattering by a single cylinder proposed in Yates and Wang [11]. Comparisons show reasonable agreement between the present results and those (both numerical and experimental) of Yates and Wang [11]. For this test case, the solitary wave was correctly generated and the free surface elevations at various measuring points were well reproduced by the present model. The horizontal wave forces on the cylinder were also reasonably predicted for various amplitude solitary waves. The numerical model was then used to investigate a solitary wave interacting with a group of eleven cylinders. Complex hydrodynamic processes involving violent wave-wave and wave-structure interaction tend to occur in this case. The model is capable of handling such complex 3D scenarios.

ACKNOWLEDGEMENTS

This research was funded by the University of Bath (Graduate school funding, sponsor code: 3451) and HR Wallingford (internal research project: DDY0485). This research made use of the Balena High Performance Computing Service at the University of Bath. The first author gratefully thanks both institutions for sponsoring his PhD study. DMK acknowledges the support of the IHRC at FIU.

REFERENCES

[1] Chen L., Sun L., Zang J. et al. Numerical study of roll motion of a 2-D floating structure in viscous flow [J]. Journal of Hydrodynamics, 2016, 28(4): 544-563.
[2] Rogers, B.D., Dalrymple, R.A., and Stansby, P.K. Simulation of caisson breakwater movement using 2-D SPH[J], Journal of Hydraulic Research, 2010, 48, 135-141.
[3] Harlow, F.H. The Particle-In-Cell Computing Method For Fluid Dynamics[M], in Methods in Computational Physics, B. Alder, Editor. Academic Press: New York. 1964, 319-343.
[4] Brackbill, J.U. and Ruppel, H.M. FLIP: A Method for Adaptively Zoned, Particle-in-Cell Calculations of Fluid Flows in Two Dimensions[J], Journal of Computational Physics, 1986, 65(2), 314-343.
[5] Zhu, Y.N. and Bridson, R. Animating sand as a fluid[J], Acm Transactions on Graphics, 2005, 24(3), 965-972.
[6] Kelly, D.M. Full particle PIC modelling of the surf and swash zones[C], in Proc. 33rd Int. Conf. Coast. Eng., Santander, Spain, 2012.
[7] Kelly, D.M., Chen, Q., and Zang, J. PICIN: A Particle-in-Cell Solver for Incompressible Free Surface Flows with Two-Way Fluid-Solid Coupling[J], Siam Journal on Scientific Computing, 2015, 37(3), B403-B424.
[8] Chen, Q., Kelly, D.M., Dimakopoulos, A.S., and Zang, J. Validation of the PICIN solver for 2D coastal flows[J], Coastal Engineering, 2016, 112, 87-98.
[9] Chen, Q., Zang, J., Dimakopoulos, A.S., Kelly, D.M., and Williams, C.J.K. A Cartesian cut cell based two-way strong fluid-solid coupling algorithm for 2D floating bodies[J], Journal of Fluids and Structures, 2016, 62, 252-271.
[10] Chen, Q., Zang, J., Kelly, D.M., and Dimakopoulos, A.S. A 3D parallel Particle-In-Cell solver for wave interaction with vertical cylinders[J], Under Review by Ocean Engineering, Unpublished results.
[11] Yates, G.T. and Wang, K.H. Solitary Wave Scattering by a Vertical Cylinder: Experimental Study[J], Proceedings of the Fourth (1994) International Offshore and Polar Engineering Conference, 1994, Vol III, 118-124.
[12] Zhao, M., Cheng, L., and Teng, B. Numerical simulation of solitary wave scattering by a circular cylinder array[J], Ocean Engineering, 2007, 34(3-4), 489-499.
[13] Ai, C.F. and Jin, S. Non-hydrostatic finite volume model for non-linear waves interacting with structures[J], Computers & Fluids, 2010, 39(10), 2090-2100.
[14] Mo, W.H. and Liu, P.L.F. Three dimensional numerical simulations for non-breaking solitary wave interacting with a group of slender vertical cylinders[J], International Journal of Naval Architecture and Ocean Engineering, 2009, 1(1), 20-28.
[15] Kagemoto, H., Murai, M., and Fujii, T. Second-order resonance among an array of two rows of vertical circular cylinders[J], Applied Ocean Research, 2014, 47, 192-198.
[16] Harlow, F.H. and Welch, J.E. Numerical Calculation of Time-Dependent Viscous Incompressible Flow of Fluid with Free Surface[J], Physics of Fluids, 1965, 8(12), 2182-2189.
[17] Chorin, A.J. Numerical solution of the Navier-Stokes equations[J], Mathematics of computation, 1968, 22, 745-762.
[18] Gibou, F., Fedkiw, R.P., Cheng, L.T., and Kang, M.J. A second-order-accurate symmetric discretization of the Poisson equation on irregular domains[J], Journal of Computational Physics, 2002, 176(1), 205-227.
[19] Ng, Y.T., Min, C., and Gibou, F. An efficient fluid-solid coupling algorithm for single-phase flows[J], Journal of Computational Physics, 2009, 228(23), 8807-8829.
[20] Edwards, E. and Bridson, R. A high-order accurate particle-in-cell method[J], International Journal for Numerical Methods in Engineering, 2012, 90(9), 1073-1088.
[21] Ralston, A. Runge-Kutta methods with minimum error bounds[J], Mathematics of computation, 1962, 16(80), 431-437.
[22] Chen, Q. Development of A Full Particle PIC Method for Simulating Nonlinear Wave-Structure Interaction[D], Ph.D. Thesis, Bath, University of Bath, 2017.
[23] Wu N. J., Tsay T. K., Chen Y. Y. Generation of stable solitary waves by a piston-type wave maker [J]. Wave Motion, 2014, 51(2): 240-255.
[24] Wu, N.J., Hsiao, S.C., Chen, H.H., and Yang, R.Y. The study on solitary waves generated by a piston-type wave maker[J], Ocean Engineering, 2016, 117, 114-129.
[25] Goring, D.G. Tsunamis--the propagation of long waves onto a shelf[D], Ph.D. Thesis, California Institute of Technology, 1978.
[26] Fenton, J. A ninth-order solution for the solitary wave[J], Journal of fluid mechanics, 1972, 53(2), 257-271.
[27] Cao, H.J. and Wan, D.C. RANS-VOF solver for solitary wave run-up on a circular cylinder[J], China Ocean Engineering, 2015, 29(2), 183-196.